10.1098/rspa.2001.0920

THE ROYAL SOCIETY

Vortex instability from a near-vertical heated surface in a porous medium II. Nonlinear evolution

By D. Andrew S. Rees

Department of Mechanical Engineering, University of Bath, Claverton Down, Bath BA2 7AY, UK

Received 4 July 2001; accepted 24 September 2001; published online 14 May 2002

We consider the nonlinear evolution of vortex instabilities in a near-vertical free convection boundary layer in a porous medium. At such inclinations, both small amplitude and strongly nonlinear disturbances may be described within the confines of boundary-layer theory with no further approximations. Steady vortices are induced by placing a thermal disturbance within the boundary layer and by computing their development downstream using a parabolic solver.

It is found that the strength of the resulting convection depends not only on the wavelength of the vortex disturbance, but also on the amplitude of the disturbance and its point of introduction into the boundary layer. Whenever vortices grow, they attain a maximum strength before decaying once more. Curiously, there is a specific disturbance amplitude that yields the largest possible response downstream, in the sense that both smaller and larger initial amplitudes yield weaker responses. This unusual phenomenon is shown to be related to the shape of the vortex.

Keywords: vortex instabilities; nonlinear theory; porous media; boundary layer

1. Introduction

In Rees (2001), which will be referred to as part I, we undertook a detailed linearized stability analysis of free convective boundary-layer flow from a uniform-temperature heated surface embedded in a porous medium. Attention was focused on the near-vertical case where the inclination from the vertical is taken to be asymptotically small. Although this seems to be an unusually specific configuration to consider, it has the advantage that the full vortex disturbance equations may be described within the boundary-layer approximation. It is also quite likely that many of the qualitative features uncovered here, in part I and in subsequent papers, will also apply at more realistic angles from the vertical.

Vortex disturbances are characterized by their spanwise wavenumber and their cross-stream profile. In common with many other boundary-layer flows, the neutral stability curve exists only for wavenumbers below a certain maximum value. For disturbances with wavenumbers above this value, boundary-layer flows are predicted to be linearly stable, which means that small amplitude perturbations should always decay as they travel downstream. At wavenumbers below the maximum value, disturbances may grow, although they decay initially if they have been introduced

relatively close to the leading edge. However, it was shown in part I that such a neutral curve, which is computed only after assuming the streamwise variation of the disturbance, is too restrictive. The evolution of disturbances was shown to be governed by a parabolic system of equations whose numerical solution demonstrated that disturbances may begin to grow at stations closer to the leading edge than are given by the neutral curve. This conclusion was based on a thermal energy of the vortex as a measure of the strength of the disturbance.

The main aim of this paper is to extend the analysis of part I into the nonlinear regime. It was shown in part I that the fully nonlinear evolution of vortex disturbances may also be modelled within the framework of the boundary-layer approximation and is also described by a parabolic system. This system is now three dimensional, unlike the linearized disturbance equations, and its solution is effected by means of a spanwise Fourier decomposition and the application of the well-known Keller-box method (Keller & Cebeci 1971) in a slightly unusual form.

In view of the above discussion, it is not surprising to find that the detailed evolution of a vortex disturbance depends on its wavenumber, but we find that it also depends very strongly on where it has been introduced into the boundary layer and on its amplitude. Details of how the evolution depends on these factors are complicated, but, in general, when the wavenumber is below the maximum value on the neutral curve, vortices experience growth over a range of values of x, the streamwise coordinate. In some instances, this is preceded by decay, but it is also succeeded by decay, which is a surprising result, since a local Darcy–Rayleigh number based on the boundary-layer thickness continues to increase with distance from the leading edge, and therefore one would expect the boundary layer to be increasingly susceptible to instability. Another surprising result is obtained by considering the response of the boundary layer to disturbances of various amplitudes. In this case, the maximum vortex strength increases as the amplitude of the initial disturbance increases, but there is a maximum response that is such that further increases in the strength of the initial disturbance serves only to decrease the eventual local response of the boundary layer. A reason for this is discussed later. A similar scenario also occurs when the point of introduction of the disturbance is varied.

The outline of the paper is as follows. In § 2 we present the governing equations, which were derived in part I, and describe the numerical method used to solve them. The numerical results are presented in § 3 and are discussed in detail. Finally, in § 4 the implications of this work are discussed.

2. Governing equations and numerical method

We consider how vortex instabilities evolve along the free convection boundary-layer flow induced by a near-vertical uniform-temperature heated surface embedded in a porous medium. The detailed flow configuration and coordinate system are sketched in figure 1. In common with part I, we assume that the surface is asymptotically close to being vertical, but still upward facing, since in that limit the full disturbance equations satisfy the boundary-layer approximation; at $O(1)$ angles from the vertical streamwise diffusion become important and it will prove necessary to undertake an elliptic fully three-dimensional unsteady numerical analysis. But, in the present case, vortex evolution, even in the fully nonlinear regime, may be studied by means of solving a set of parabolic partial differential equations.

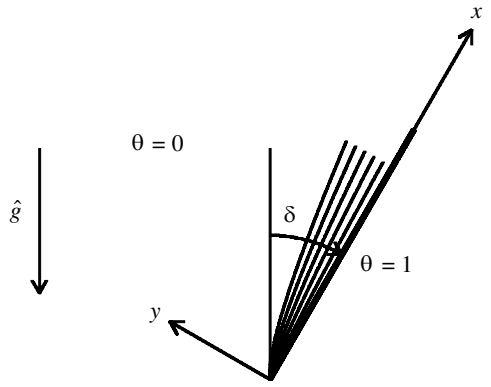

Figure 1. Sketch of the flow domain and boundary conditions.

The detailed derivation of the full disturbance equations subject to the boundary-layer approximation has been given in part I and will not be repeated here. It was shown that the perturbation pressure, p, and the perturbation temperature, θ, satisfy the equations

$$p'' + \xi^2 p_{zz} = \tfrac{1}{2}(\xi\theta_\xi - \eta\theta') + \xi\theta', \tag{2.1}$$

$$\theta'' + \xi^2\theta_{zz} = (\tfrac{1}{2}f')\xi\theta_\xi - (\tfrac{1}{2}f)\theta' + (f'')(\xi - \tfrac{1}{2}\eta)\theta - (f'')p' + \tfrac{1}{2}(\xi\theta_\xi - \eta\theta')\theta + \xi\theta\theta' - p'\theta' - \xi^2 p_z\theta_z, \tag{2.2}$$

subject to

$$p' = \theta = 0 \quad \text{at } \eta = 0 \quad \text{and} \quad p, \theta \to 0 \quad \text{as } \eta \to \infty, \tag{2.3}$$

where $\eta = y/x^{1/2}$ is the similarity variable, $\xi = x^{1/2}$ is a scaled streamwise coordinate and (x, y, z) forms a non-dimensional Cartesian coordinate system in the streamwise, cross-stream and spanwise directions, respectively. Furthermore, subscripts denote derivatives with respect to the corresponding variables and primes denote derivatives with respect to η in common with many other non-similar analyses. The stream function, ψ, corresponding to the basic boundary-layer flow, is given by $\psi = x^{1/2}f(\eta)$, and both the vertical velocity and the temperature by $f'(\eta)$, where f satisfies the following equation and boundary conditions:

$$f''' + \tfrac{1}{2}ff'' = 0, \quad f(0) = 0, \quad f'(0) = 1 \quad \text{and} \quad f' \to 0 \quad \text{as } \eta \to \infty. \tag{2.4}$$

These were first derived and solved by Cheng & Minkowycz (1977). As equations (2.1) and (2.2) form a parabolic system of partial differential equations, initial conditions are required to complete the specification of the problem. Precise details of these are given in the following section.

In part I, solutions of the linearized version of equations (2.1) and (2.2) were obtained using the Keller-box method. In this numerical technique, the full equations are reduced to first-order form in η, discretized using central difference approximations based halfway between grid points in both the η- and ξ-directions, and the resulting nonlinear system of difference equations solved using a multi-dimensional version of the Newton–Raphson iteration scheme, the iteration matrix having block-tridiagonal form. In the present paper, the governing equations have an extra z-dependence, which makes the numerical difficulties much greater. We have solved

the system (2.1) and (2.2) by taking a truncated spanwise Fourier expansion in the form

$$p(\xi,\eta,z) = \tfrac{1}{2}p_0(\xi,\eta) + \sum_{n=1}^{N} p_n(\xi,\eta)\cos nkz, \tag{2.5}$$

$$\theta(\xi,\eta,z) = \tfrac{1}{2}\theta_0(\xi,\eta) + \sum_{n=1}^{N} \theta_n(\xi,\eta)\cos nkz, \tag{2.6}$$

where k is the wavenumber of the primary vortex and N is the truncation level of the series. In the simulations we present here, a value of $N = 5$ was used; this was deemed to be sufficient, as the amplitude of the fifth term ($n = 5$) always remained very considerably smaller than that of the primary vortex ($n = 1$). The substitution of (2.5) and (2.6) into equations (2.1) and (2.2) is straightforward, but lengthy to present and therefore we omit this detail. We obtain a system of $2N + 2$ second-order parabolic partial differential equations in ξ and η to solve. With $N = 5$, this means that the standard Keller-box implementation uses 24 variables when reduced to first-order form in η, and hence the block-tridiagonal iteration matrix is composed of 24×24 submatrices. Such a system was programmed initially, but its execution was very slow. Therefore, we elected to keep the equations in second-order form and to use central differences in η based on the grid points. This has various consequences. (i) The block-tridiagonal structure of the iteration matrix is retained, which means that the same basic code may be used. (ii) The submatrices are now 12×12, which results in a very considerable increase in the speed of the code. (iii) The method retains second-order accuracy in η in terms of the computed values of p and θ. (iv) Derived values, such as the surface rate of heat transfer, now become of first-order accuracy in η, as such quantities rely on taking numerical derivatives.

We also elected, as in part I, to use backward difference approximations in ξ. One reason for this is to eliminate pointwise oscillations, which sometimes occur when using central differences (see Rees (1997) for an example of where the use of backward differences was also essential). One advantage of its use is that it is not necessary to specify an initial profile for p. To see this, we first note that no ξ derivatives of p occur in either equation (2.1) or (2.2). This means that p is defined only in terms of θ and θ_ξ. Therefore, a disturbance may be introduced by specifying only the θ profile, and, given that a backward difference method has been employed, we do not need to rely on the p profile at the point of introduction of the disturbance in order to march the numerical solution on to the next ξ gridpoint.

As with many other parabolic boundary-layer simulations by the present author, we use numerical derivatives to compute the iteration matrix from the definition of the 'right-hand-side' vector. This has the distinct advantage of a much reduced development time for the numerical code, which, given the complexity of the system being studied here, is very considerable, although the execution time is necessarily increased.

In general, we set

$$\theta_1 = A\eta \mathrm{e}^{-\eta} \quad \text{at } \xi = \xi_0, \tag{2.7}$$

where we refer to A as the amplitude of the vortex disturbance and ξ_0 as the point of introduction of the disturbance. In all the computations presented here, we have used 50 equally spaced gridpoints lying in the range $0 \leqslant \eta \leqslant 10$; this maximum value

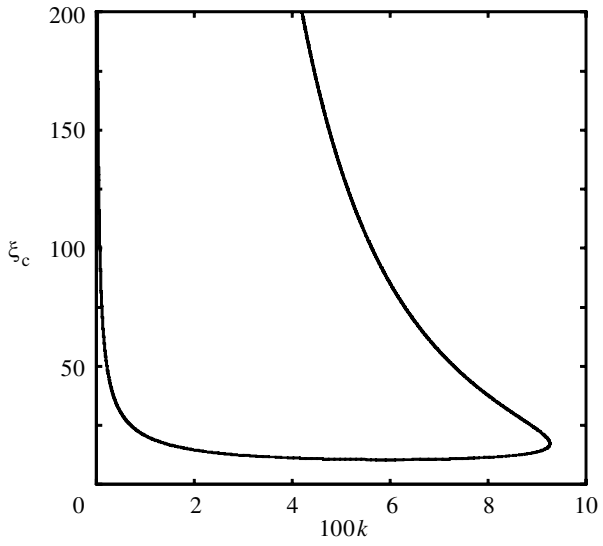

Figure 2. Neutral stability curve: ξ_c against k.

of η is sufficient to contain the evolving disturbances, which, as will be seen later, have a slight tendency to become concentrated towards the heated surface. Uniform steps of length 0.1 in the ξ-direction were also used.

3. Numerical results

In figure 2 we reproduce, for reference, the neutral curve obtained from the approximate stability analysis undertaken in part I. The main reason for this is to allow the following nonlinear results to be interpreted in terms of a linearized stability theory, albeit one that is approximate. We see from this figure that vortex disturbances will always decay whenever k is greater than *ca.* 0.0924, whereas at smaller values of k, infinitesimally sized disturbances may expect to enjoy growth within a range of values of ξ, although this range is both preceded and succeeded by decay. Our aim is to investigate numerically how nonlinearities affect this scenario.

(*a*) *Some typical cases*

We begin by highlighting the general behaviour of some typical cases before moving on to a more comprehensive description of how the vortex evolution changes with amplitude, A, and point of introduction of the disturbance, ξ_0.

In figure 3 we display the detailed evolution of the primary vortex ($n = 1$), its harmonics ($n > 1$) and the mean correction to the basic flow ($n = 0$) as ξ varies. Here we have used $k = 0.04$, $\xi_0 = 8$ and $A = 0.1$ as representative values of k, ξ_0 and A. At this value of k, the numerical data corresponding to figure 2 indicates that infinitesimally sized disturbances should grow when $\xi > 10.66$ or, equivalently, when $x > 113.7$, and will begin to decay again when $\xi \simeq 132.74$ or $x \simeq 17\,620$. The curves displayed in figure 3 show the evolution with ξ of the surface rates of heat transfer due to each Fourier mode; these are given by $q_n = \partial\theta_n/\partial\eta|_{\eta=0}$ ($0 \leqslant n \leqslant 5$) and are fairly typical of those obtained when $k < 0.094$ and when ξ_0 is below the

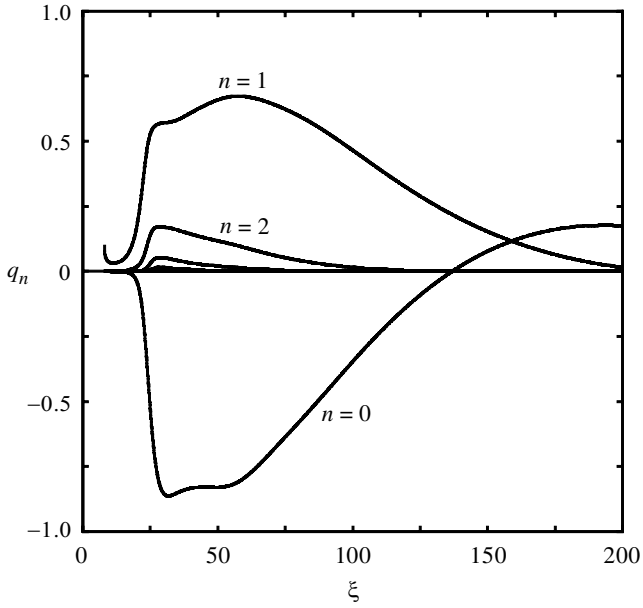

Figure 3. Variation with ξ of the surface rates of heat transfer, q_n, corresponding to the various Fourier modes, $n = 0, 1, 2 \ldots$. We have taken $\xi_0 = 8$, $k = 0.04$ and $A = 0.1$.

neutral curve. The amplitude of the primary vortex, as represented by q_1, first decays until ξ is near to the first neutral value, and then it begins to grow. For this case, the growth continues until ξ is just above 50, at which point the amplitude slowly decays; this value of 50 is substantially below the restabilizing value of 220.9 read off the data plotted in figure 2 at $k = 0.04$. One purpose of the rest of our results is to explain this discrepancy between the infinitesimal-amplitude results of figure 2 and the large-amplitude simulation.

It is important to note that the mean correction to the basic flow ($n = 0$) gives an increase in the overall rate of heat transfer from the surface as the mean local rate of heat transfer becomes more negative. Secondly, the $n = 2$ curve is significant only over a small range of values of ξ and that higher modes do not contribute greatly to the local rate of heat transfer; this observation, which is common to all our simulations, justifies the use of $N = 5$ for the number of modes used.

Figure 4 shows how the cross-section of the vortex pattern varies with distance from the leading edge. Here we show contours of the perturbation isotherms at selected values of ξ, where, in each subframe, the contours are scaled to lie between $\pm\theta_{\mathrm{extr}}$, where the extremum value satisfies

$$\theta_{\mathrm{extr}} = \max(\theta_{\max}, -\theta_{\min}). \tag{3.1}$$

As ξ increases, the vortices begin to grow in strength and eventually the vortices that correspond to negative perturbation temperatures (the middle vortex in each subframe of figure 4) begin to acquire a triangular profile, while the neighbouring vortices rise from the surface. At this point, the boundary layer becomes thicker, but eventually the vortex system weakens, which results in the 'negative' vortex becoming smaller and becoming progressively more confined to the near-wall region.

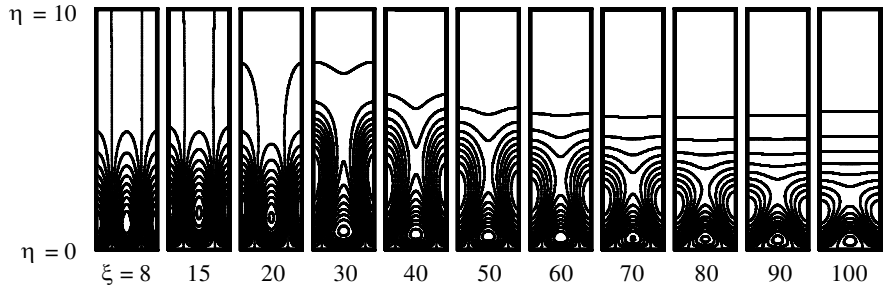

Figure 4. Cross-section of the vortex system corresponding to the perturbation temperature profile for various values of ξ. This vortex system was obtained using $\xi_0 = 8$, $k = 0.05$ and $A = 0.1$.

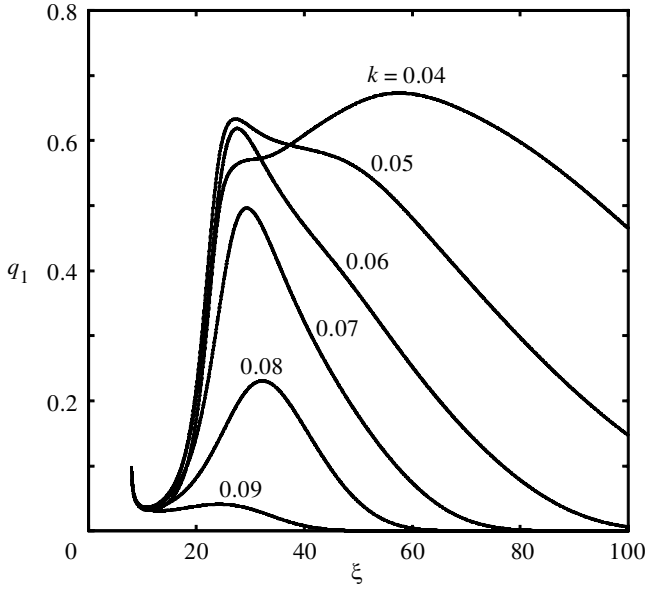

Figure 5. The variation in the surface rate of heat transfer, q_1, due to the primary vortex for various wavenumbers. We have taken $\xi_0 = 8$ and $A = 0.1$.

A comparison between the boundary-layer responses for different vortex wavenumbers is depicted in figures 5 and 6, for otherwise identical cases. We have taken $\xi_0 = 8$ and $A = 0.1$ for these figures. Figure 5 shows how q_1, the surface rate of heat transfer due to the primary vortex, evolves with ξ. All the curves show an initial decrease in the vortex strength, since $\xi_0 = 8$ is in the stable region shown in figure 2 for all wavenumbers. Thereafter, the vortex grows in amplitude, but the distance over which this behaviour is maintained depends very much on the vortex wavenumber, and subsequently the vortex decays. For $k = 0.09$, this region of growth is relatively short, which is consistent with the small region of instability indicated in figure 2, and therefore the vortex does not grow greatly. On the other hand, when $k < 0.08$, the initial growth is relatively rapid. The vortex quickly undergoes a nonlinear saturation, which inhibits further growth and causes decay, at least in terms of the surface rate of heat transfer, even though the values of ξ and k lie within the unstable region

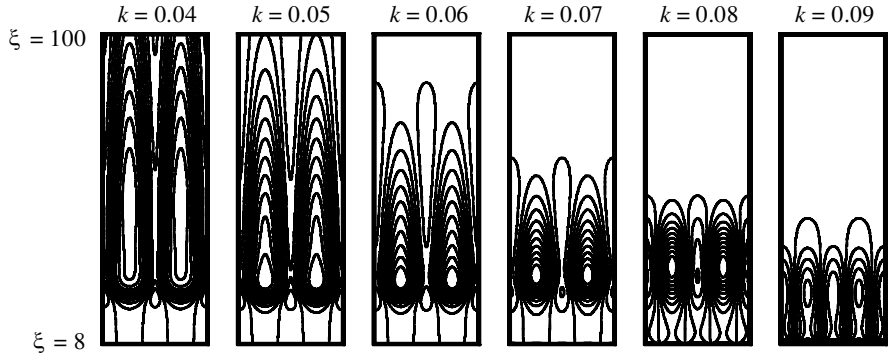

Figure 6. Isolines of the surface rate of heat transfer over four vortices in (ξ, z)-space for various values of the vortex wavenumber, k. Again we have taken $\xi_0 = 8$ and $A = 0.1$. The horizontal coordinate varies between $z = 0$ and $z = 4\pi/k$.

delimited by the neutral curve given in figure 2. This phenomenon will be considered in more detail later.

An alternative view of the overall vortex structure is shown in figure 6. Contours of the surface rate of heat transfer, $\partial\theta/\partial\eta|_{\eta=0}$, in the ξ, z-plane for each of the cases shown in figure 5 are given. Each part shows two periods in the z-direction, i.e. four vortices. When $k = 0.09$, the four vortices shown are of roughly the same strength, as is indicated by the fact that $\theta_{\max}$ is almost the same as $-\theta_{\min}$, and both the growth and decay phases of the evolution are evident. As the wavenumber decreases, the vortices become increasingly strong, and nonlinear effects serve to favour one vortex over its nearest neighbours. That this must be so may be gleaned from a careful consideration of figure 3; the $n = 1$ curve corresponds to $\cos kz$, while the $n = 0$ curve is the change in the mean heat transfer due to the presence of vortices. Therefore, at some values of z ($z = 0$, for example), the local rate of heat transfer from the mean correction and from the primary vortex almost cancel each other out, since $\theta_1'(\eta = 0)$ and $\theta_0'(\eta = 0)$ have opposite signs. But at other values of z ($kz = \pi$, for example), they reinforce each other. The effect on the surface rate of heat transfer is that the four vortices appear to become just two, a phenomenon that is particularly strong for $k = 0.04$ and $k = 0.05$. In reality, the four vortices still exist, and each alternate vortex lifts itself away from the surface, as is seen in figure 4.

(*b*) *The effect of varying the disturbance amplitude, A*

Even with the introductory results presented so far, it is clear that nonlinearity plays an important role in the detailed evolution of the vortex. Therefore, this subsection is devoted to a survey of how the amplitude of the initial disturbance affects the subsequent development of the flow. We have chosen to use the amplitudes $A = 10^{-1}, 10^{-2}, 10^{-3}, \ldots, 10^{-20}$. As above, the vortex wavenumbers vary in steps of 0.01, from 0.04 to 0.09. We have again chosen to use the point $\xi_0 = 8$ at which to introduce the disturbance; the effect of using other values of ξ_0 is considered in the next subsection. From a numerical point of view, the presence of amplitudes as small as 10^{-20} necessitates the use of a relative convergence criterion in the numer-

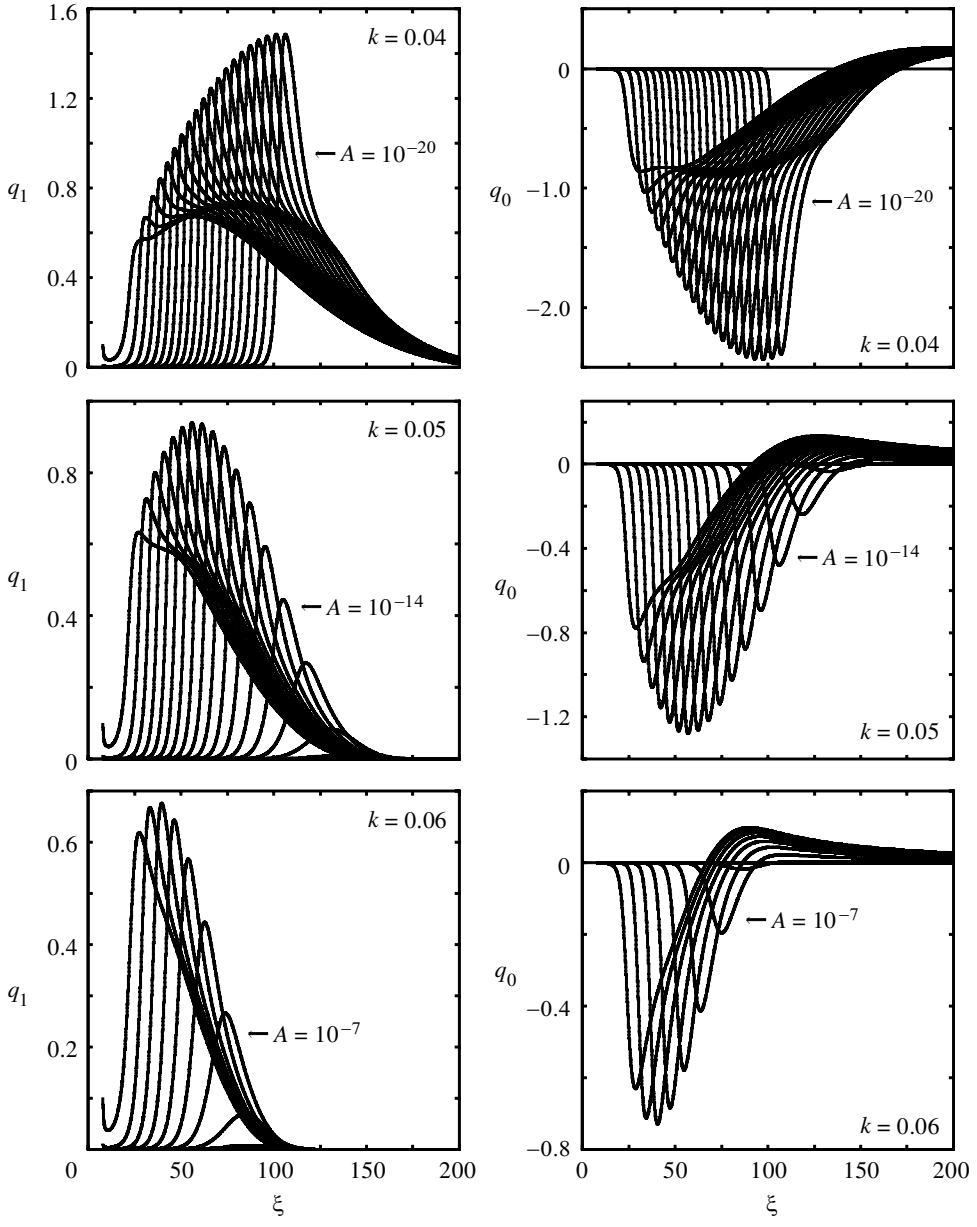

Figure 7. The variation with ξ of q_1 (left-hand figure parts) and q_0 (right-hand figure parts) for various wavenumbers between $k = 0.04$ and $k = 0.09$ and amplitudes $A = 10^{-1}, 10^{-2}, \ldots, 10^{-20}$. The value $\xi_0 = 8$ was used. The curve on the extreme left corresponds to $A = 10^{-1}$ in each case.

ical code, rather than an absolute one, in order to ensure that the evolving solution has converged to a sufficient number of significant figures at each value of ξ.

The detailed surface rates of heat transfer for the primary vortex (q_1) and the mean correction to the basic heat transfer (q_0) are given in figure 7. In each part, the range of values of ξ on the abscissa is always the same, but the scale used for the

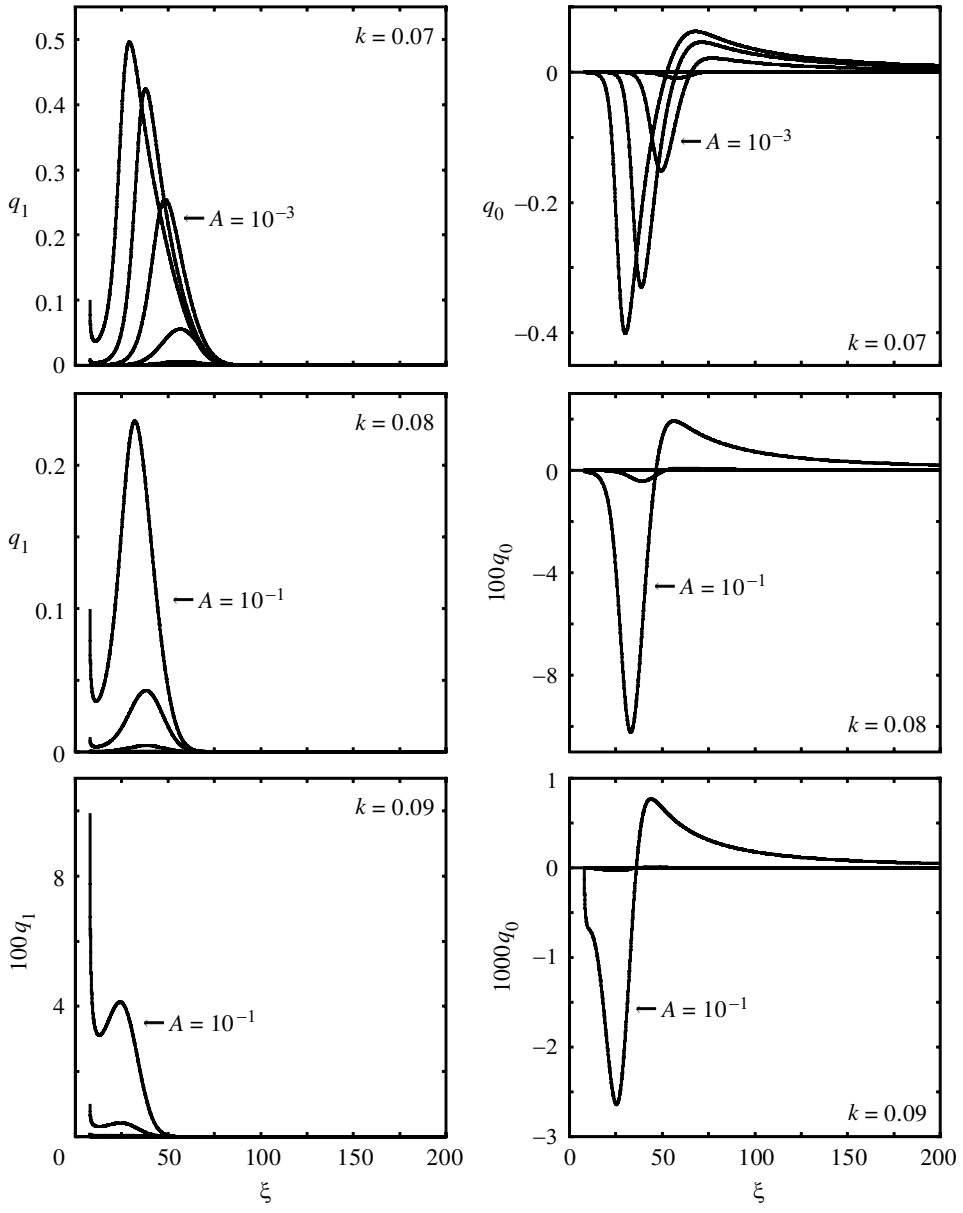

Figure 7. (*Cont.*) The variation with ξ of q_1 (left-hand figure parts) and q_0 (right-hand figure parts) for various wavenumbers between $k = 0.04$ and $k = 0.09$ and amplitudes $A = 10^{-1}$, $10^{-2}, \ldots, 10^{-20}$. The value $\xi_0 = 8$ was used. The curve on the extreme left corresponds to $A = 10^{-1}$ in each case.

ordinate (i.e. for the heat transfer) varies from case to case. The heat transfer due to the primary vortex appears on the left of each pair. The detailed numerical results indicate that the onset of convection (defined here as the point at which $\partial q_1/\partial \xi = 0$) occurs at roughly the same value of ξ for any chosen wavenumber and it is therefore almost independent of the initial amplitude of the disturbance. However, the value of

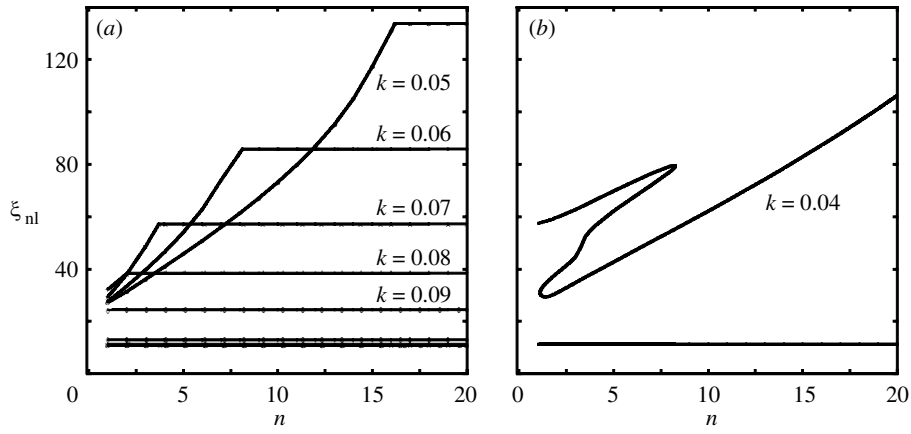

Figure 8. Variation in the values of the nonlinear neutral points, ξ_{nl}, with $n = -\log_{10} A$ for different vortex wavenumbers. The lines placed near to $\xi_{\mathrm{nl}} = 11$ correspond to onset of instability, while the others correspond to the beginning of decay.

ξ at which the heat transfer begins to decrease again is a very strong function of the initial amplitude. For all values of k, the value of ξ at which the peak heat transfer occurs seems to increase as the initial amplitude of the disturbance decreases. This may be understood in terms of the fact that a relatively large distance is required for the vortex initiated by a relatively small amplitude disturbance to develop to nonlinear saturation.

Perhaps more surprising is the fact that, for each wavenumber, there is a maximum local response in terms of q_1, and that these maxima can occur for very small initial amplitudes. For $k = 0.04$, for instance, the peak local response corresponds to $A \simeq 10^{-19}$, whereas $A \simeq 10^{-7}$ when $k = 0.05$. A similar variation with A of the local maximum mean response (q_0) occurs, although the peak responses occur at slightly different values of A. Intuitively, one would expect the amplitude of the response to a disturbance to increase monotonically with increasing disturbance amplitudes, but the detailed results presented here indicate otherwise, suggesting that there is a more subtle interplay between the magnitude of A and local growth rates.

The right-hand graphs in figure 7 correspond to q_0. In all cases, q_0 becomes negative, at least initially, and very strongly so for the smaller wavenumbers, thereby substantially increasing the local mean rate of heat transfer. However, at the larger values of ξ, when the primary vortex has reduced in strength quite considerably, q_0 becomes positive. This is a universal phenomenon, but the largest positive value attained never causes the mean heat transfer ($\frac{1}{2}q_0 + f''(0)$) to become positive.

In all the graphs shown in figure 7, the peak local heat transfer occurs at or below the corresponding upper branch value of ξ depicted in figure 2. For the larger wavenumbers ($k = 0.07$, 0.08 and 0.09), this is seen very clearly since the distance over which linear growth is predicted by figure 2 is relatively small, and comparison of the parts comprising figure 7 shows a rapidly decreasing region where the disturbance grows as k increases.

In figure 8 we summarize the stability characteristics displayed in figure 7 by showing the values of ξ at which $\mathrm{d}q_1/\mathrm{d}\xi$ changes sign as a function of the disturbance amplitude; this value we denote by ξ_{nl} and refer to by the name *nonlinear neutral point*. More precisely, if n is defined by $A = 10^{-n}$, then we show how the value

of ξ_{nl} varies with n at the point where q_1 takes extreme values. Figure 8*a* shows the variation of ξ_{nl} for $k \geqslant 0.05$, while figure 8*b* gives the $k = 0.04$ curve, which is more complicated. As mentioned earlier, q_1 attains its minimum values when ξ is very close to the lower branch of the neutral stability curve given in figure 2. But the values of ξ_{nl} clearly increase as n increases, again as mentioned before, but this figure also shows that there is a limit to that increase; there is an abrupt change from a monotonically increasing variation with n to a constant, and this constant lies just slightly above the neutral curve given in figure 2. In this regard, the constant corresponds to those values depicted in the linear stability analysis of part I, and the point at which the abrupt change in slope takes place corresponds to that value of A above which nonlinear effects become significant. Thus we see that the lower wavenumbers are increasingly responsive to very small amplitude disturbances. When $k = 0.04$, however, there is a qualitative change in the shape of the ξ_{nl}, n curves as they become multivalued. This occurs only for the larger disturbance amplitudes, and the four values of ξ_{nl} that correspond to $n = 2$ (or $A = 10^{-2}$) may be seen to correspond to the four extrema in the $A = 10^{-2}$ curve in the $k = 0.04$, q_1 figure part of figure 7.

Finally, it is necessary to mention the fact that the detailed curves presented in figures 7 and 8 vary with the shape of initial disturbance and with the value of ξ_0 at which the disturbance is introduced. Although we do not consider variations in the disturbance shape in the present paper, variations in ξ_0 are described in the next subsection.

(*c*) *The effect of varying* ξ_0

Now we turn our attention to a survey of how the boundary layer responds to disturbances introduced at different values of ξ_0 for different wavenumbers. Variations of q_1 with ξ are displayed in figure 9 for $A = 0.1$, for the same set of wavenumbers as in figure 7, and for ξ_0 varying in steps of 1, from 1 to 15, in steps of 5, from 15 to 100, and steps of 10, from 100 to 200. In all cases, the value of q_1 decays whenever $\xi < 10$, but the point at which growth first occurs (ξ_{nl}) depends strongly on both ξ_0 and k. An example of the dependence on ξ_0 is shown in figure 10, which corresponds to $k = 0.06$, a typical case. We see that ξ_{nl} is independent of ξ_0 when $\xi_0 \leqslant 5$, but ξ_{nl} then begins to increase as ξ_0 increases above 5. This is related to the fact that the disturbance profile given in (2.7) is not precisely that which gives the fastest growth. For relatively small values of ξ_0, the disturbance evolves over a relatively large distance, which allows it to attain a shape that corresponds at least roughly to that with the largest growth rate, and therefore ξ_{nl} is essentially independent of ξ_0. Conversely, for larger values of ξ_0, an ideal shape for growth has not yet been attained and therefore the disturbance needs to evolve beyond that given by the linear stability analysis of part I.

Whenever ξ_0 lies between the lower and upper branches of the neutral stability curve given in figure 2, the value of q_1 shown in figure 9 decays at first, but only for a very short distance before growth occurs. This may also be explained by appealing to the fact that the initial disturbance does not correspond to the one that is ideal for growth. Thus it is possible to vary the length of this short region of decay by altering the shape of the disturbance from that given in (2.7); when it is more like the shape given by the linear stability analysis, then the region is shorter, but when the profile has multiple signs, for example, then the region is lengthened.

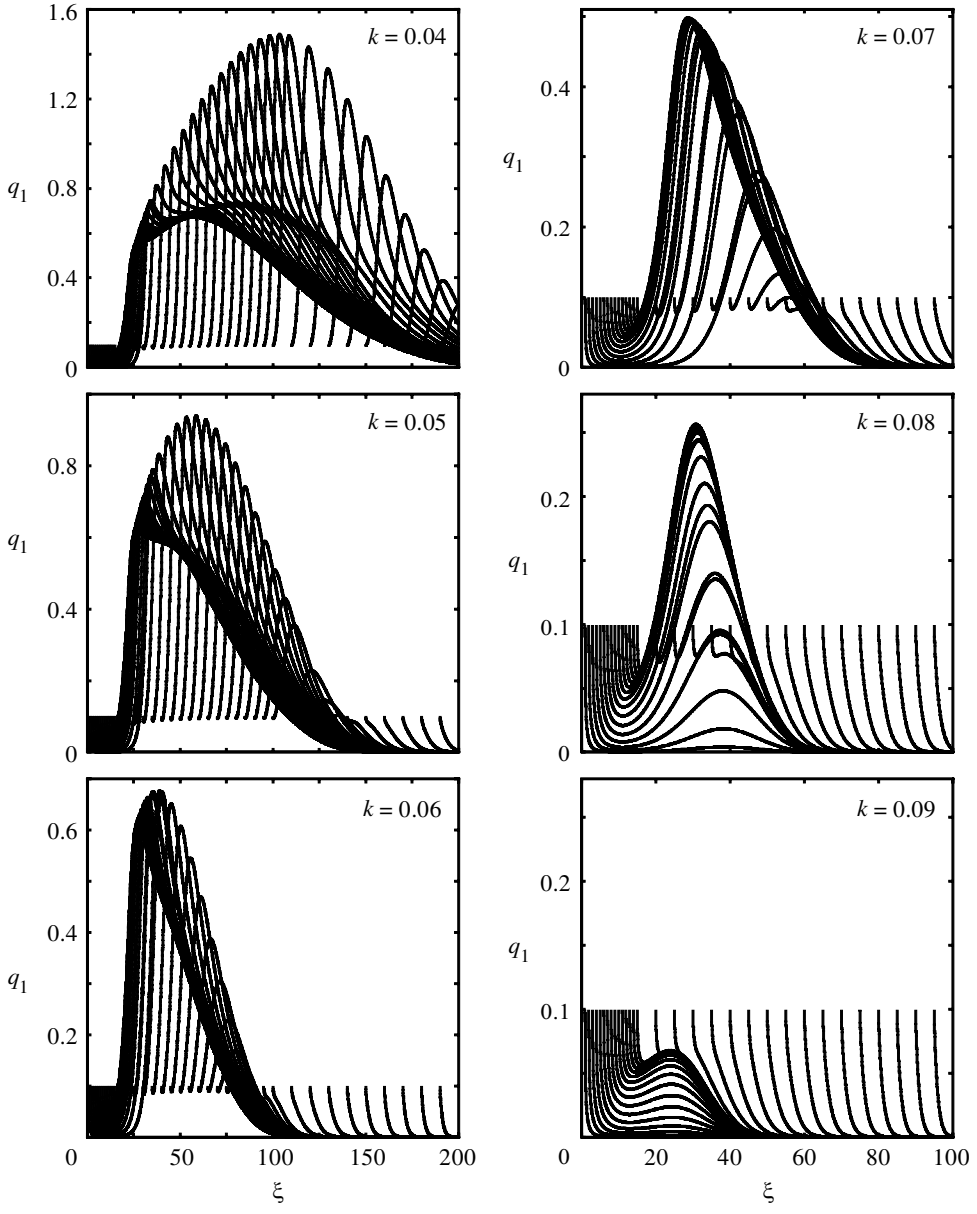

Figure 9. The variation of q_1 with ξ for various values of ξ_0 with each figure part depicting different vortex wavenumbers between $k = 0.04$ and $k = 0.09$. In each case $A = 0.1$ is the initial vortex amplitude.

Figure 9 also clearly shows the fact that different values of ξ_0 also yield different peak values of q_1. For example, for $k = 0.04$, the largest value of q_1 is attained when $\xi_0 \simeq 95$. Likewise, it shows that decay occurs prematurely when the flow is highly nonlinear. This is particularly evident when considering the peaks in q_1 for $k \leqslant 0.07$. For larger wavenumbers, such as $k = 0.09$, the variation in the value of ξ at which q_1 is a maximum is much more gentle.

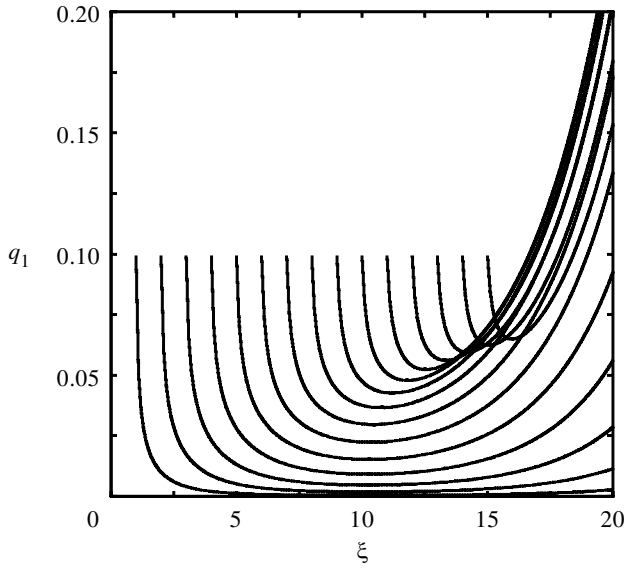

Figure 10. A close-up view of the $k = 0.06$ figure part of figure 9. The solid circles denote where the slope of q_1 against ξ is zero, and marks the onset of instability.

These features are summarized in figure 11, which shows how $\xi_{\rm nl}$ varies with ξ_0. In all the parts of figure 11, the horizontal lines correspond to the onset of convection and the re-establishment of stability, as given by the approximate linear analysis of part I, while the diagonal line is given by $\xi_{\rm nl} = \xi_0$, and therefore nonlinear onset must be above this line. For $k = 0.09$, the linearized stability analysis is followed closely, even though $A = 0.1$ represents quite a large disturbance. Thus nonlinear onset occurs slightly below the linear onset value given in part I, but then rises once $\xi_0 \geqslant 9$, to lie just above the $\xi_{\rm nl} = \xi_0$ line. The value of $\xi_{\rm nl}$ corresponding to the re-establishment of stability lies just above the appropriate linear stability value.

As k decreases from 0.09, there begins to be a distinctive change in the shape of the curve corresponding to the re-establishment of stability. In particular, the curve develops a increasingly marked dip as k decreases, again indicating that the value of q_1 is beginning to decay prematurely. Once more, when k is as low as 0.04, the evolving disturbance exhibits multiple regions of growth and decay, and the variation of $\xi_{\rm nl}$ with ξ_0 becomes more complicated.

The curves shown in figure 11 represent the situation that pertains when the disturbance profile is given by (2.7) and when $A = 0.1$. It is again true that the shape of the curves depends on the disturbance profile, but the variation with A is very marked, since nonlinearities play a crucial role. Therefore, we display in figure 12 the $\xi_{\rm nl}$ curves corresponding to $k = 0.06$ for $A = 10^{-1}$, 10^{-3}, 10^{-5}, 10^{-7} and 10^{-9} in order to see how the re-establishment of stability depends on the disturbance amplitude. We note first that there is no significant variation in the values of $\xi_{\rm nl}$ at onset. But there is a monotonic rise in the distance over which growth is maintained as A decreases. For this wavenumber, the linearized analysis predicts the stability boundaries very adequately when $A \leqslant 10^{-9}$, but does not do so when A is substantially larger than this.

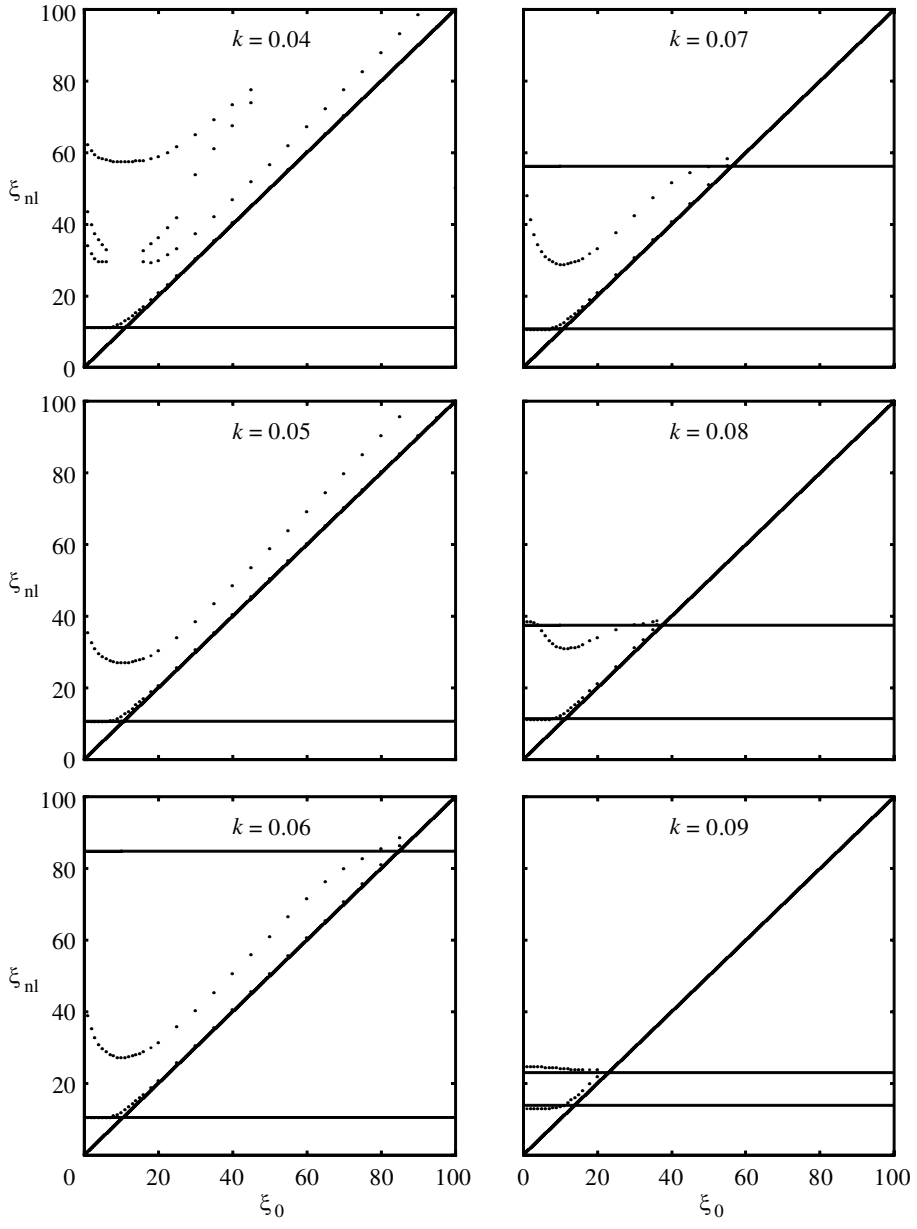

Figure 11. The variation of ξ_{n1} with ξ_0 for various values of the vortex wavenumber. The amplitude of the initial disturbance is $A = 0.1$. The horizontal lines depict the linear stability criteria given in figure 2, while the diagonal line shows where $\xi_{n1} = \xi_0$.

4. Conclusions

In this paper we have sought to give a fairly comprehensive overview of the nonlinear response of the thermal boundary layer in porous media to vortex disturbances. One reason for this is that the present work represents the first nonlinear vortex study in porous medium thermal boundary-layer flows; the fairly extensive litera-

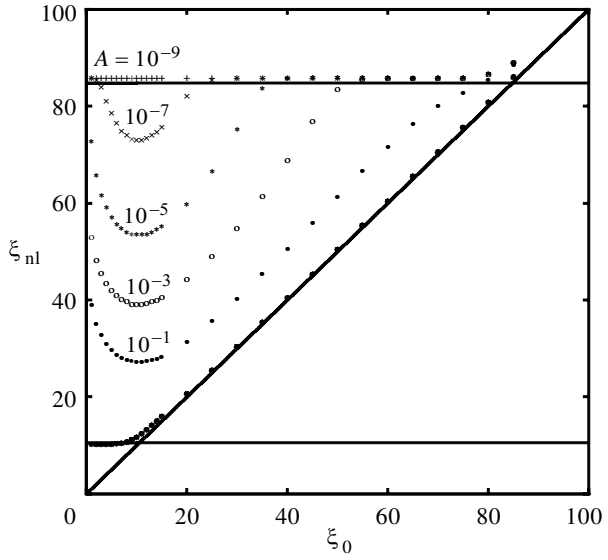

Figure 12. The effect of different disturbance amplitudes, A, on the nonlinear stability criterion for $k = 0.06$.

ture on linearized vortex theory has been reviewed by Rees (1998). Attention has been restricted to the admittedly idealized configuration of a heated surface that is asymptotically close to the vertical, but the equations governing the nonlinear vortex evolution are parabolic within this regime, which greatly simplifies what would otherwise have been an unsteady three-dimensional elliptic simulation. In particular, we have varied the vortex wavenumber, k, the position of introduction of the disturbance, ξ_0, and the amplitude, A. We have not presented any quantitative results showing how the disturbance shape affects the evolution of the vortices.

It is clear that nonlinear effects alter substantially many aspects of the flow from what they are when linearized theory is valid. These include the values of ξ at which vortices begin to grow and decay (as exemplified by figures 8 and 11), the shape of the vortices (figure 4), and the rather unusual dependence of the peak rate of heat transfer on the amplitude and position of the disturbance (figures 7 and 9, respectively). All of these features may be explained by recourse to relatively straightforward notions involving growth rates, distances over which disturbances may grow, the evolution of the disturbance profiles with ξ and their shape relative to that given by linear theory.

One further feature that is worthy of emphasis is the fact that all such vortex disturbances eventually decay. Although one might naively expect growth to continue, since the local Rayleigh number based on the boundary-layer thickness continues to grow, and hence it would seem to indicate that the boundary layer is becoming increasingly unstable, the increasing thickness of the boundary layer also causes the aspect ratio of the vortex to decrease, an effect that stabilizes disturbances. In this context, as with many other growing boundary layers such as Blasius flow over a flat plate and the vertical clear fluid boundary layer from a vertical hot surface, stabilization occurs as the vortex evolves downstream.

Notwithstanding this, the boundary layer continues to grow in thickness and becomes more unstable, and therefore we would expect the decaying vortices presented here eventually to be destabilized themselves by disturbances of other forms. At present, there is no experimental evidence to back up even the linearized theory, let alone secondary nonlinear instabilities. In the context of the thermal boundary layer induced in a clear fluid by a hot inclined surface, Chen *et al*. (1991) undertook a weakly nonlinear theory based on the parallel flow approximation to show that it is possible for a vortex system like that given here to undergo a subharmonic instability that effectively doubles the wavelength of the vortices. Some further and very recent confirmation of this mechanism has been given by Jeschke & Beer (2001). Preliminary calculations using the code described herein confirm that the present vortex system also undergoes this wavelength-doubling instability; it is hoped to give a detailed report on this aspect in due course, although some preliminary results are given in Rees (2002).

A second candidate for a possible instability mechanism is the Eckhaus instability. This was analysed in detail for the weakly nonlinear Bénard problem by Newell & Whitehead (1969), who showed that it too modifies the wavelength of convection cells. It is too early to state categorically that this mechanism is important in the present problem. A third possibility is that the flow might become unsteady, in which case the present solution methodology would be inadequate to model the consequences. That unsteadiness is a possible mechanism that may be justified by analogy with the onset of unsteady convection in the Darcy–Bénard problem, as reviewed by Kimura (1998). For a convection cell of a unit aspect ratio in a uniform horizontal layer, unsteady flow occurs at a Rayleigh number, R, of approximately 390, and that the mechanism is destabilization with respect to two-dimensional travelling waves in the upper and lower thermal boundary layers which appear within the main convecting cell at that Rayleigh number. The onset of steady Darcy–Bénard convection takes place at $R_{\mathrm{c}} = 4\pi^2$, and therefore unsteady convection occurs at a Rayleigh number of approximately $10R_{\mathrm{c}}$. If this is translated very crudely into the present problem, then it indicates that we could expect unsteady effects in the form of waves travelling around the vortices at a value of ξ near to 100, since the local Rayleigh number is proportional to $x^{1/2} = \xi$ and the onset of vortices is close to $\xi = 10$.

It is hoped that many of the results presented here might be applicable to boundary layers at more moderate angles of inclination. However, the nature of the flow changes from parabolic to elliptic at such inclinations, and it is likely that there will be a much reduced dependence of the vortex system on the amplitude and shape of the initiating disturbance.

References

Chen, C. C., Labhari, A., Chang, H.-C. & Kelly, R. E. 1991 Spanwise pairing of finite-amplitude longitudinal vortex rolls in inclined free convective boundary layers. *J. Fluid Mech.* **231**, 73–111.

Cheng, P. & Minkowycz, W. J. 1977 Free convection about a vertical flat plate imbedded in a porous medium with application to heat transfer from a dike. *J. Geophys. Res.* **82**, 2040–2044.

Jeschke, P. & Beer, H. 2001 Longitudinal vortices in a laminar natural convection boundary-layer flow on an inclined flat plate and their influence on heat transfer. *J. Fluid Mech.* **432**, 313–339.

Keller, H. B. & Cebeci, T. 1971 Accurate numerical methods for boundary layer flows. 1. Two dimensional flows. In *Proc. Int. Conf. Numerical Methods in Fluid Dynamics*. Lecture Notes in Physics. Springer.

Kimura, S. 1998 Onset of oscillatory convection in a porous medium. In *Transport phenomena in porous media* (ed. D. B. Ingham & I. Pop), pp. 77–102. Oxford: Pergamon.

Newell, A. C. & Whitehead, J. A. 1969 Finite bandwidth, finite amplitude convection. *J. Fluid Mech.* **38**, 279–303.

Rees, D. A. S. 1997 Three-dimensional free convection boundary layers in porous media induced by a heated surface with spanwise temperature variations. *Trans. ASME J. Heat Transfer* **119**, 792–798.

Rees, D. A. S. 1998 Thermal boundary layer instabilities in porous media: a critical review. In *Transport phenomena in porous media* (ed. D. B. Ingham & I. Pop), pp. 233–259. Oxford: Pergamon.

Rees, D. A. S. 2001 Vortex instability from a near-vertical heated surface in a porous medium. I. Linear instability. *Proc. R. Soc. Lond.* A **457**, 1721–1734.

Rees, D. A. S. 2002 Recent advances in the instability of free convection boundary layers in porous media. In *Transport phenomena in porous media II* (ed. D. B. Ingham & I. Pop). (In the press.)